RESEARCH ARTICLE

Title:

The impact of dwell time on the contextual effect of visual and passive lead-in movements

Abbreviated title:

Impact of dwell time on contextual lead-in movements

Laura Alvarez-Hidalgo[1], David W. Franklin[2,3,4] & Ian S. Howard[1*]

[1] School of Computing, Engineering and Mathematics, University of Plymouth, Plymouth, Devon, United Kingdom.
[2] Neuromuscular Diagnostics, Department of Sport and Health Sciences, Technical University of Munich, Bavaria, Germany.
[3] Munich Institute of Robotics and Machine Intelligence (MIRMI), Technical University of Munich, Bavaria, Germany.
[4] Munich Data Science Institute (MDSI), Technical University of Munich, Bavaria, Germany.

Correspondence should be addressed to: ISH: ian.howard@plymouth.ac.uk

Telephone: +44 1752 586324

Journal Section: Behavioral/Cognitive

Number of pages: 34

Number of figures: 12

Number of tables: 2

Number of words for abstract: 229

Number of words for introduction: 554

Number of words for discussion: 1178

Statement of Financial Interests or Conflicts of Interest: The authors declare that they have no financial, personal, or professional interests that could be construed to have influenced the paper.

Acknowledgements: Financial support for LAH was provided by the Engineering and Physical Sciences Research Council (EPSRC), and The University of Plymouth. Financial support for ISH was provided by The University of Plymouth. During the preparation of this work, the last author (ISH) utilized ChatGPT-4o for proofreading.

Keywords: Dynamic learning; Lead-in context; Temporal decay; Motor memory; Predictive compensation.

ABSTRACT (229/250)

Contextual cues arising from distinct movements are crucial in shaping control strategies for human movement. Here, we examine the impact of visual and passive lead-in movement cues on unimanual motor learning, focusing on the influence of “dwell time”, in which two-part movements are separated by the interval between the end of the first movement and the start of the second. We used a robotic manipulandum to implement a point-to-point interference task with switching opposing viscous curl-fields in male and female human participants. Consistent with prior research, in both visual and passive lead-in conditions, participants showed significant adaptation to opposing dynamics with short dwell times. As dwell time increased for both visual and passive signals, past movement information had less contextual influence. However, the efficacy of visual movement cues declined faster as dwell times increased. At dwell times greater than 800ms, the contextual influence of prior visual movement was small, whereas the effectiveness of passive lead-in movement was found to be significantly greater. This indicates that the effectiveness of sensory movement cues in motor learning is modality-dependent. We hypothesize that such differences may arise because proprioceptive signals directly relate to arm movements, whereas visual inputs can relate to many aspects of movement in the environment and not just to our own arm movements. Therefore, the motor system may not always find them as relevant for predictive control of dynamics.

Significance Statement (114/120)

This study reveals the critical role of contextual cues from distinct movements in shaping motor learning. Here, we examined the influence of “dwell time”, the interval between the end of the first and the start of the second movement. Notably, visual lead-in movement cues lose their effectiveness sooner than passive lead-in movement cues as dwell time increases. This is possibly due to their lesser relevance to self-generated movements and the longer processing delays in visual information. This finding underscores the modality-dependent nature of sensory cues in motor learning. Understanding these effects can inform the development of more effective rehabilitation and training programs by leveraging the strengths of different sensory modalities to optimize motor learning.

News & Noteworthy (74/75)

This research uncovers, for the first time, how visual and proprioceptive sensory cues affect motor learning as a function of the pause or "dwell time" in two-part movements. The study has shown that visual lead-in movement cues lose their effectiveness sooner than passive lead-in movement cues as dwell time increases. By revealing the modality-dependent nature of sensory information, this study enhances our understanding of motor control and opens new possibilities for improving therapeutic interventions.

INTRODUCTION (554)

To perform effective arm movements, the human motor system must adapt to both the arm's dynamics and its environment. Numerous studies have investigated how the motor system deals with changes in dynamics. Viscous curl-fields, in particular, have proven to be useful for examining the adaptation of the human motor system to novel dynamics (1–3). In untrained participants, a curl-field initially disrupts straight hand movements by exerting a force perpendicular to the hand motion and proportional to its velocity. However, adaptation to curl-field dynamics occurs rapidly, usually over a few dozen movement trials. After this period, movement trajectories almost resemble those executed when no curl-field is present. This adaptation, however, is hindered when the direction of the curl-field changes unpredictably. When individuals experience two opposing viscous curl-fields during movements, the learning from the second can disrupt the memory of the first. This phenomenon is known as retrograde interference (4, 5). Similarly, prior learning can affect subsequent learning, a phenomenon known as anterograde interference (6–8). When curl-fields with opposing directions are presented randomly and in balanced proportions, during so-called interference tasks, it has been observed that learning does not occur unless contextual cues are present (9–13).

This interference paradigm provides a valuable technique for testing the impact of contextual information. With effective contextual cues, learning to adapt to opposing curl-fields becomes possible. Prior lead-in movements have been shown to significantly influence the learning of novel dynamics (14–18). Their influence has also been demonstrated in bimanual tasks, extending the understanding of lead-in movements across both arms (19, 20). Notably, in the unimanual case, visual, passive, and active lead-in movements all exert a substantial contextual effect on the adaptation to novel dynamics in subsequent movements (14).

The generalization characteristics of unimanual lead-in movements have been extensively studied across various modalities. These studies include examining the effects of movement direction in visual (17, 21), passive (15), and active lead-ins (16). In terms of prior movement direction, active and passive lead-ins show similar angular generalization characteristics, whereas those of visual lead-ins are broader and weaker. Furthermore, the examination of generalization for additional kinematic movement characteristics, such as distance, speed, or duration, reveals notable differences between visual and passive lead-in movements (18). Another related study found that increased variability in active lead-ins slowed motor adaptation, whereas variations in visual lead-ins had no significant effect (22). It was suggested that this phenomenon could be explained by the differences between their respective generalization characteristics. Taken together, these variations indicate that the way the motor system receives information from past movements significantly affects the formation of motor memory and its recall.

Another noteworthy aspect of active lead-in movements is the reduction in their effect as dwell time increases, disappearing almost completely over 1000 milliseconds (14). Given

that different lead-in modalities exhibit varying generalization characteristics, this suggests that the influence of dwell time on adaptation might also vary. Although the impact of dwell time in active lead-ins has been studied in some detail, the behaviors of passive and visual lead-ins under similar conditions have not yet been fully examined. In this study, we investigate the impact of dwell time on the contextual effects of visual and passive lead-ins in the learning of opposing dynamics, examining how these effects diminish as dwell time increases.

MATERIALS AND METHODS

Participants: We recruited 48 human participants, each randomly assigned to two distinct experiments, with three different dwell time conditions. The first group, consisting of 24 participants (14 females and 10 males, average age: 20.83 ± 1.99 years), participated in Visual Lead-in Experiment 1. The second group, consisting of 24 participants (10 females and 14 males, average age: 21.92 ± 3.23 years), took part in Passive Lead-in Experiment 2.

According to the Edinburgh Handedness Questionnaire (23), all participants were right-handed. Prior to their involvement, participants were not informed of the study's specific objectives, and each participant provided informed written consent. All experiments were conducted in full accordance with a protocol approved by the Science and Engineering Faculty Research Ethics and Integrity Committee at the University of Plymouth, and we strictly adhered to the approved guidelines.

Apparatus: All experiments were conducted using a vBOT planar robotic manipulandum, paired with a 2D virtual reality system (24), as illustrated in Fig. 1. The handle's location was determined using optical encoders, sampled at 1000Hz. Appropriate state-dependent endpoint forces were applied to the handle by controlling the torque of the robot’s drive motors.

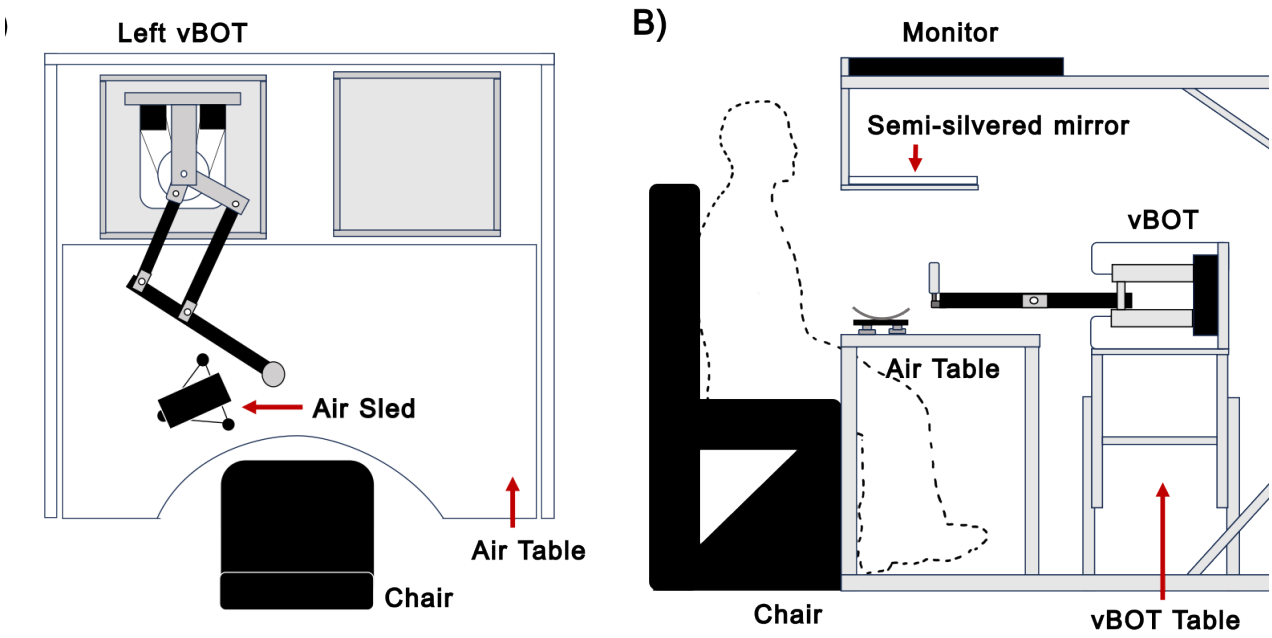

Figure 1. Schematic Illustration of the Experimental Setup. **A:** Plan view of the vBOT robotic manipulandum, air table, and air sled. **B:** Side view of the vBOT robotic manipulandum, showing its virtual reality environment.

A force transducer (Nano 25; ATI), mounted beneath the handle, measured the applied forces. The output signals were low-pass filtered at 500Hz using 4th-order analog Bessel filters prior to digitization. To minimize body movement, participants were comfortably seated in a sturdy chair positioned in front of the apparatus and securely fastened to the backrest with a four-point seatbelt.

During the experiment, participants held the robot handle with their right hand, while their forearm was supported by an air sled, which restricted arm movements to the horizontal plane. Participants could not see their arm or hand directly; instead, they were provided with accurate visual feedback using the virtual reality system. Images of the starting point, via-point, and target locations (each with a 1.25cm radius), as well as a hand cursor (a 0.5cm radius red disk), were overlaid to align with the actual plane and location of the participant's hand. Data were collected at a sampling rate of 1000Hz and stored on an SSD for offline analysis using MATLAB (The MathWorks Inc., Natick, MA, USA).

Force Fields

All trials began with a lead-in movement to provide context, followed by an active adaptation movement to a final target. In the adaptation phase, participants made reaching movements in three different types of trials: null field trials, viscous curl force field trials (25, 26), or simulated channel trials (27–29). The velocity-dependent viscous curl-field was implemented according to Equation (1):

$$\begin{bmatrix} F_x \\ F_y \end{bmatrix} = b \begin{bmatrix} 0 & -1 \\ 1 & 0 \end{bmatrix} \begin{bmatrix} \dot{x} \\ \dot{y} \end{bmatrix} \quad (1)$$

In this equation, the field constant b had a value of ±13Ns/m, where its sign determined the curl-field direction (clockwise or counterclockwise). Each participant was subjected to both directions of the curl-field, which were consistently linked with a specific lead-in movement direction. To minimize potential directional bias, the association between the contextual movement direction and the curl-field direction was counterbalanced across participants.

Mechanical channel trials, from the central location to the final target, were used to assess the level of predictive compensation for the curl-fields (27). These channels were implemented using a spring constant of 6,000N/m and a viscous damping constant of 30Ns/m, with their effects applied perpendicularly to the direction of motion throughout the movement. A channel trial was implemented according to Equation (2):

$$\begin{bmatrix} F_x \\ F_y \end{bmatrix} = 6000 \begin{bmatrix} -1 & 0 \\ 0 & 0 \end{bmatrix} \begin{bmatrix} x \\ y \end{bmatrix} + 30 \begin{bmatrix} -1 & 0 \\ 0 & 0 \end{bmatrix} \begin{bmatrix} \dot{x} \\ \dot{y} \end{bmatrix} \quad (2)$$

Two separate experiments were conducted with different groups of participants. In the Visual Lead-in Experiment 1, participants observed a cursor moving from a starting position towards a via-point. In contrast, in the Passive Lead-in Experiment 2, participants were pulled from a starting position to the via-point by the robotic system, requiring no active movement generation. Participants then performed a 12cm active movement to the target in both experiments.

Visual Lead-in Experiment 1:

Protocol

A schematic depiction of the experimental protocol experienced by a participant is illustrated in Fig. 2. This outlines the training and testing procedures, highlighting the directions used for both contextual and adaptation movements.

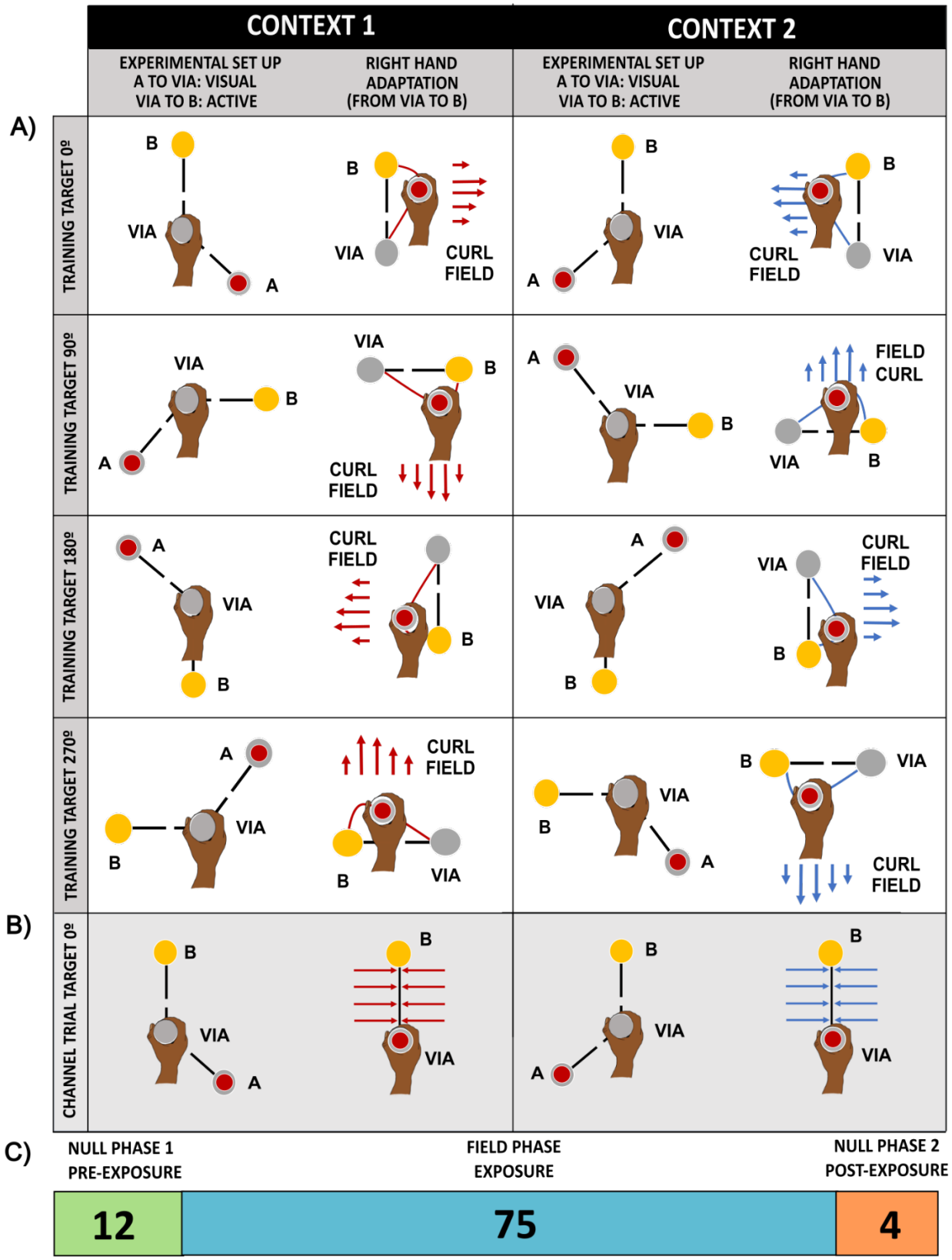
CONTEXT 1
CONTEXT 2
EXPERIMENTAL SET UP
A TO VIA: VISUAL
VIA TO B: ACTIVE
RIGHT HAND
ADAPTATION
(FROM VIA TO B)
A)
TRAINING TARGET 0º
TRAINING TARGET 90º
TRAINING TARGET 180º
TRAINING TARGET 270º
B)
CHANNEL TRIAL TARGET 0º
B
VIA
A
CURL
FIELD
FIELD
CURL
C)
NULL PHASE 1
PRE-EXPOSURE
FIELD PHASE
EXPOSURE
NULL PHASE 2
POST-EXPOSURE
12
75
4

Figure 2. Visual Lead-in Movements Experimental Design. **A**: Null and Training Trials. Each trial session began with the participant's hand at the via-point, and a grey disc indicating the starting point. After the hand remained stationary at this location for 300ms, grey and yellow discs appeared indicating the locations of the via-point and final target, respectively. At the same time, a red cursor appeared at the contextual movement's starting point and began moving towards the via-point. After the cursor reached the via-point and waited there for a designated dwell time, an acoustic beep and a simultaneous change of the via-point disc to white prompted the participant to make an active adaptation movement to the final target point. Overall, for each of the two curl-field directions, there were four different movement orientations associated with the starting locations (45°, 135°, 225°, and 315°), with each start location associated with a unique target location (0°, 90°, 180°, and 270°). This led to eight configurations in total. **B:** Channel Trials. These only used a single adaptation movement direction to a target point at 0°, associated with two visual lead-in directions, one for each curl-field direction, with starting points at 135° and 225°. **C.** Outline of the trials in the visual lead-in experimental protocol. This schematic indicates the number of blocks of trials in the null, exposure, and washout phases of the experiment. This protocol is followed in both the visual and passive lead-in experiments.

In total, there were four different starting points for the contextual movement. These were located on the circumference of a circle with a 10cm radius, with its center corresponding to the central workspace coordinate position (0, 0). Specifically, the start locations were positioned at angles of 45°, 135°, 225°, and 315°. The endpoint for the contextual movement was always at the via-point, also located at the central workspace coordinate position.

For the adaptation movement, there were four target points, located on the circumference of a circle with a 12cm radius with its center again corresponding to the central workspace coordinate position. This time, the target locations were positioned at angles of 0°, 90°, 180°, and 270°. Each adaptation movement direction was associated with two distinct contextual movement directions. These relationships determined the direction of the viscous curl-field experienced by participants during the adaptation phase of a trial. This resulted in eight unique combinations of contextual and adaptation movements, as outlined in Table 1.

Channel trials were conducted exclusively for movements toward the 0° target. The corresponding lead-in contextual movements originated from locations at either 135° or 225°.

Table 1. Specification of contextual and adaptation movements and curl-field directions. The table provides the specific combinations of adaptation target angles and contextual starting point angles used in the experiments. It also shows their corresponding

relationship between these angles and the direction of the curl-field. In a given experiment and dwell time condition, the label 'Normal' indicates the curl-field direction for four participants, and 'Reverse' represents the direction for the remaining four participants. This counterbalancing approach was used to minimize potential biases that might arise from the interaction between the direction of movement and the curl-field.

Adaptation target	Contextual start	Field direction Normal	Field direction Reverse
0°	135°	CCW	CW
0°	225°	CW	CCW
90°	315°	CCW	CW
90°	225°	CW	CCW
180°	45°	CCW	CW
180°	315°	CW	CCW
270°	135°	CCW	CW
270°	45°	CW	CCW

Set-up for a trial began with the participant holding the robotic handle and pressing the activation switch. Then, they were pulled by the robotic arm to the handle starting location of the experiment, in this case the via-position. At this stage, a grey disk was shown at the location of the starting point of the contextual movement. Once the handle remained stationary within its via-point location for 300ms, the trial proceeded.

Then, grey and yellow discs, representing the via-point and target point respectively, appeared simultaneously with a red moving cursor, which provided the contextual visual movement. The cursor moved into the central via-point following a minimum jerk trajectory.

When the contextual movement was finished, its starting location changed from grey to white, accompanied by an auditory beep. After a set dwell time at the via-point, the via-point turned white, prompting the participant to actively move to the final target. This ensured that after the contextual movement, participants remained at the via-point for a required dwell time before making the adaptation movement.

The trial terminated when the participant actively moved the cursor into the yellow target and stayed there for 300ms.

Experimental Block Design

An experiment consisted of blocks of 18 trials, each comprising 16 field trials and 2 clamp trials. During the field trials, all of the four targets were presented twice, in both opposing field directions. Each experiment began with 12 blocks of null field trials at the specified experimental dwell time relationship, allowing participants to acclimatize to making movements using the robotic manipulandum. This was followed by a training session consisting of 75 blocks of velocity-dependent curl-fields, in which the field direction was determined by the direction of the contextual movement. The experiment concluded with 4 blocks of washout trials, to examine the aftereffects of the curl-fields being removed.

Channel trials, set at the training timing relationship, were interspersed throughout the experiment.

In total, there were 1,638 trials. The study lasted around three hours, although some participants took longer in experimental conditions with longer dwell times. Participants were required to take short rest breaks every 195 to 205 trials. The exact number was determined randomly so it wouldn't lead to a trend in the data across participants at break boundaries. They could also rest at any time. The timeline of the trials in the experiment is shown in Fig. 2C.

To examine the effect of different dwell times on curl-field adaptation, groups of 8 different participants performed the experiment in three different dwell time conditions: short (~300ms), medium (~500ms), or long (~800ms). These target dwell time values were chosen based on observations from the previous dwell time study (14). The actual dwell times performed by participants were calculated from the recorded movement data trajectories, and these values were used in subsequent data analysis.

Passive Lead-in Experiment 2:

The Passive Lead-in Experiment 2 is almost identical to the Visual Lead-in Experiment 1, except for lead-in movement modality, which is passive rather than visual. A schematic depiction of the passive lead-in experimental protocol is illustrated in Fig. 3. It also displays the training and testing procedures, highlighting the four directions used for both contextual and adaptation movements.

To initiate a trial in the passive experiment, the vBOT moved the participant's hand to the starting location of the lead-in movement. At this stage, a grey disk was shown only at the location of the starting point of the contextual movement. Once the handle remained stationary within this starting location for 300ms, the trial proceeded. Then, grey and yellow discs appeared to identify the via-point and target point, respectively. The robot's handle then pulled the participant's hand to the via-point following a minimum jerk trajectory, thereby generating a passive lead-in movement. No visual cursor movement was shown during this operation to avoid the generation of visual cues. After a set dwell time at the via-point, the via-point turned white, and a red cursor appeared. The latter indicated the participant's hand position, which prompted them to actively move to the final target. The trial terminated when the actively moved cursor reached the yellow target disc and stayed there for 300ms.

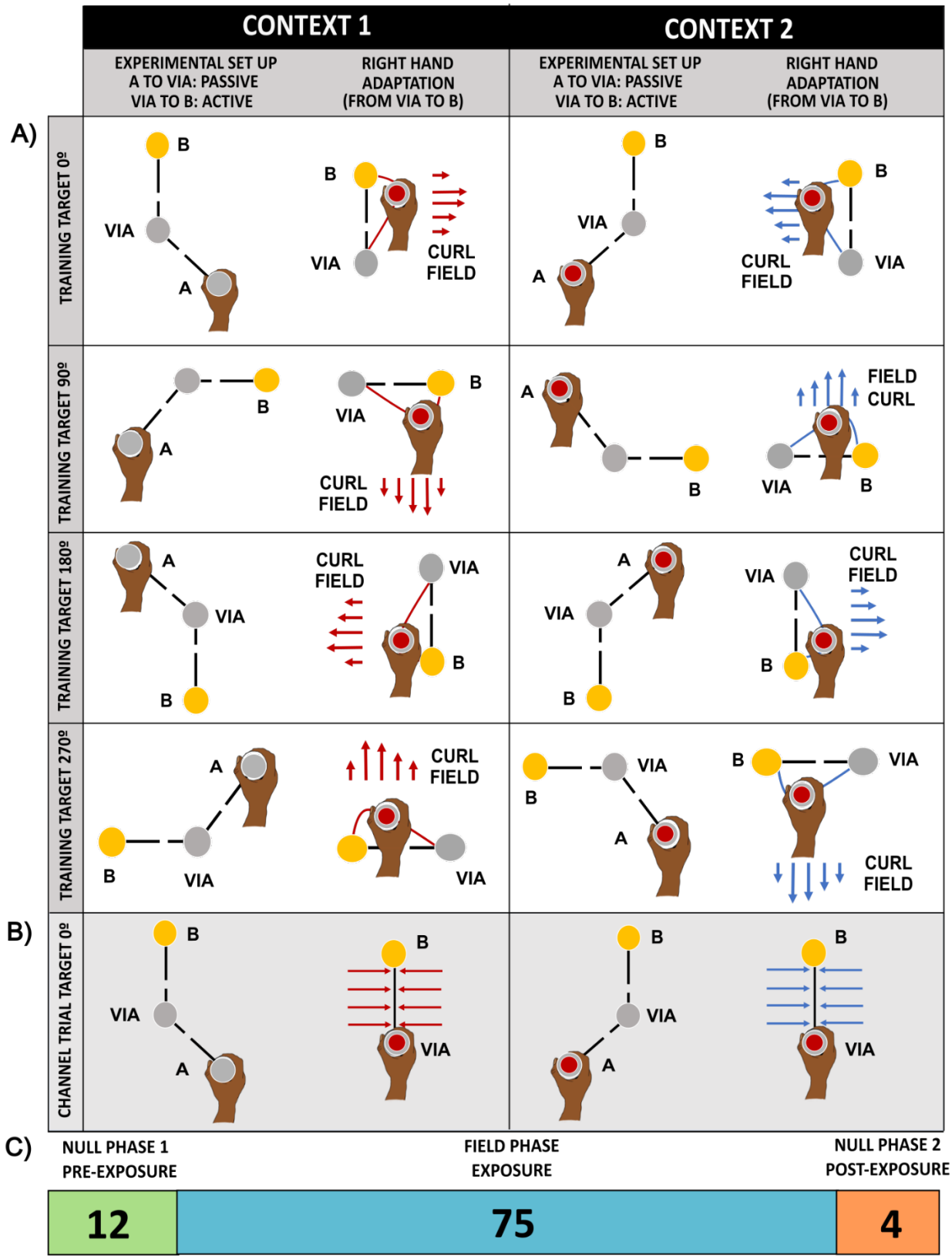
CONTEXT 1
CONTEXT 2
EXPERIMENTAL SET UP
A TO VIA: PASSIVE
VIA TO B: ACTIVE
RIGHT HAND
ADAPTATION
(FROM VIA TO B)
A)
TRAINING TARGET 0º
TRAINING TARGET 90º
TRAINING TARGET 180º
TRAINING TARGET 270º
B)
CHANNEL TRIAL TARGET 0º
B
VIA
A
CURL
FIELD
FIELD
CURL
C)
NULL PHASE 1
PRE-EXPOSURE
FIELD PHASE
EXPOSURE
NULL PHASE 2
POST-EXPOSURE
12
75
4

Figure 3. Passive Lead-in Movements Experimental Design. **A**: Null and Training Trials. Each trial session began with the participant's hand at the start point, and a grey disc indicating the starting point. After the hand remained stationary at this location for 300ms, grey and yellow discs appeared indicating the locations of the via-point and final target, respectively. At the same time, the participant's hand was guided to the via point by the robotic handle. After the hand reached the via-point and waited there for a designated dwell time, an acoustic beep, a red cursor indicating hand position, and a simultaneous change of the via-point disc to white prompted the participant to make an active adaptation movement to the final target point. Overall, for each of the two curl-field directions, there were four different movement orientations associated with the starting locations (45°, 135°, 225°, and 315°), with each start location associated with a unique target location (0°, 90°, 180°, and 270°). This led to eight configurations in total. **B:** Channel Trials. These only used a single adaptation movement direction to a target point at 0°, associated with two passive lead-in directions, one for each curl-field direction, with starting points at 135° and 225°. **C** Outline of the trials in the passive lead-in experimental protocol.

Data Analysis

The experimental data were processed offline using MATLAB R2024a. Learning was evaluated using two metrics: kinematic error during adaptation movements and force compensation during channel trials. Additionally, the actual dwell times were calculated for all participants in each experiment.

Hand Trajectory Plots

Hand trajectory plots provide a useful indication of participants' movement behavior, showing the effect of the introduction and subsequent removal of the curl-fields. In both lead-in experiments, there were four critical stages: The last block of null-field exposure, the initial block of curl-field exposure, the final block of curl-field exposure, and the initial washout block after curl-field removal.

t critical stages in the experiment, we selected hand trajectories only for the adaptation phase of each movement, excluding the channel trials. We then analysed each of these four selected blocks of trials separately. In each chosen block, there were eight different combinations of target direction and curl-field direction per participant. We calculated the mean and standard error (SE) across participants.

Kinematic Error

For each null and viscous curl-field trial, the kinematic error during the adaptation phase of the movement was quantified using its Maximum Perpendicular Error (MPE). The MPE was calculated as the maximum deviation of the hand's path from the straight line connecting the actual start position of the movement to the center of the target.

For each participant, an average MPE was first computed for all movements for each curl-field direction separately, across two blocks (16 trials for each direction). Then, the mean

and standard error (SE) of these signed MPEs were calculated across all participants and plotted to indicate behavior in each field direction.

Next, we appropriately combined the individual participants' results from clockwise (CW) and counterclockwise (CCW) field trials to obtain the overall mean and standard error (SE) of the MPE values across all participants and for both field directions, giving values corresponding to 32 field trials. In the latter calculation, the sign of the MPE was flipped appropriately so that both force field directions would produce positive errors.

Force Compensation

During channel trials, the perpendicular force exerted on the wall of the simulated channel was measured using a force transducer. This enabled the estimation of predictive feedforward adaptation by regressing measured force against the movement velocity along the channel (30). The use of a channel is often considered a more reliable method to assess learning than simply observing the reduction of kinematic error during force field adaptation, which can be influenced by muscle co-contraction (31, 32).

For each participant, an average compensation value was first computed for all movements for each curl-field direction separately, across two blocks (each with two channel trials per direction). Then, the mean and standard error (SE) of these signed compensation values were calculated across all participants and plotted to indicate behavior in each field direction.

The force compensation values were also averaged over the four consecutive channel trials in two blocks, which corresponded to both field directions. This was achieved by appropriately adjusting the sign of the values before calculating the mean. To examine the overall adaptation to the two viscous curl-fields during training, we then computed the mean and standard error (SE) of compensation for the training trials across all participants.

Estimation of Dwell Time

To estimate the actual dwell times of movements performed by participants, we calculated the time difference between the end of the lead-in movement and the start of the adaptation movement. The termination of the lead-in movement was identified using a recorded lead-in flag signal supplied from the vBOT data. After the contextual lead-in had terminated, the hand was located at the via-point in both visual and passive lead-in experimental conditions. The start of the adaptation movement was then estimated as occurring when the hand position moved away from the central via-point by more than (1.25 + 0.2) cm, which was just outside its via circle, and was traveling at a speed greater than 5cm/s. The dwell time formula is shown in Equation (3):

$$dwell\ time = \text{contextual movement end time} - \text{adaptation movement start time} \quad (3)$$

A histogram of the dwell time values across all trials in each experimental condition was generated to visualize their distribution, leading to three histograms for the Visual Lead-in Experiment 1 and another three for the Passive Lead-in Experiment 2. For each of

these six sets of histogram data, the mean and standard deviation of the dwell time values were calculated to further quantify them.

Statistical Analysis

Statistical analyses were conducted using JASP (33). To ensure the validity of our analyses, Mauchly's test was used to assess the assumption of sphericity when applicable. In cases where this assumption was violated, the degrees of freedom were adjusted using the Greenhouse-Geisser correction. The significance level (α) was set at 0.05 for all tests, and omega squared (ω^2) was reported as the effect size. Omega squared (ω^2) serves as a measure of how much variance in the dependent variable is explained by the explanatory variables.

Each of the two experiments was conducted with different participants under three dwell time conditions, resulting in a total of six sets of MPE data and six sets of force compensation data. For each of these six datasets, we first performed repeated measures ANOVAs to examine differences in MPE and force compensation at various critical phases within each experimental condition.

To evaluate kinematic error, we compared the final pre-exposure MPE (the mean of the last two pre-exposure blocks), the initial exposure MPE (the mean of the first two exposure blocks), the final exposure MPE (the mean of the last two exposure blocks), and the initial washout MPE (the mean of the first two washout blocks). This comparison was conducted using a repeated measures ANOVA, with phase serving as a repeated factor (4 levels). When a significant main effect was observed, we proceeded with post-hoc comparisons using the Holm-Bonferroni correction.

For force compensation, we compared the final pre-exposure MPE (the mean of the last pre-exposure blocks), the final exposure MPE (the mean of the last two exposure blocks), and the initial washout MPE using a repeated measures ANOVA, with phase (3 levels: pre-exposure, final exposure, and washout) as the repeated factor.

To compare MPE across dwell time conditions within each experiment, we performed ANOVAs on both the initial MPE (the mean of the first two exposure blocks) and the final exposure MPE (the mean of the last two exposure blocks), treating dwell time as a 3-level factor.

In parallel, we conducted ANOVAs on the mean of the final two exposure blocks for force compensation, with dwell time considered as a 3-level factor. Post-hoc comparisons were conducted using the Holm-Bonferroni correction whenever a significant main effect was identified.

To compare results across experiments, we performed ANOVAs on the force compensation data, specifically using the mean of the final 10 exposure blocks. In this analysis, both experiment condition (2 levels) and dwell time (3 levels) were considered as factors. Again, post-hoc comparisons were conducted with the Holm-Bonferroni correction if a significant main effect was detected.

RESULTS

Participants performed one of two experiments, one with a visual contextual lead-in, and the other with a passive contextual lead-in, to examine the effects of lead-in modality on adaptation to two opposing force fields. In both experiments, participants first experienced a contextual movement (visual or passive) to a central via-point. After a specified dwell time, they were required to perform an active movement to a given target location.

In each experiment, there were three conditions with different dwell time requirements, which were performed by different groups of participants. These permitted the examination of how adaptation to two opposing curl-fields is affected as the time delay between the contextual movement and the adaptation movement was changed.

Each experiment consisted of a baseline, in which the active movement took place in the null-field condition to acclimatize participants to the experiments and to quantify their baseline movement performance, followed by the introduction of curl force fields introduced to examine adaptation and recall of these novel dynamics (exposure phase). Finally, there was a washout phase.

Visual Lead-in Experiment 1:

Dwell Time Analysis: We first examined the dwell times performed by each participant during the exposure phase. The dwell times correspond to the measured times between the end of the contextual movements and the initiation of the corresponding adaptation movements. This analysis was performed separately for the short, medium, and long experimental conditions.

Fig. 4 shows the histogram plots for the three different dwell time conditions. Across all trials in each of these dwell time conditions (short, medium, and long), the mean ± SE values were 285.2 ± 8.5ms, 459.4 ± 7.6ms, and 806.9 ± 20.55ms, respectively. In addition, their mean and mode values differ from each other, and the mode of the distributions are shifted from the mean to the left, towards lower values. The dwell time distributions become more spread out for the larger dwell time conditions.

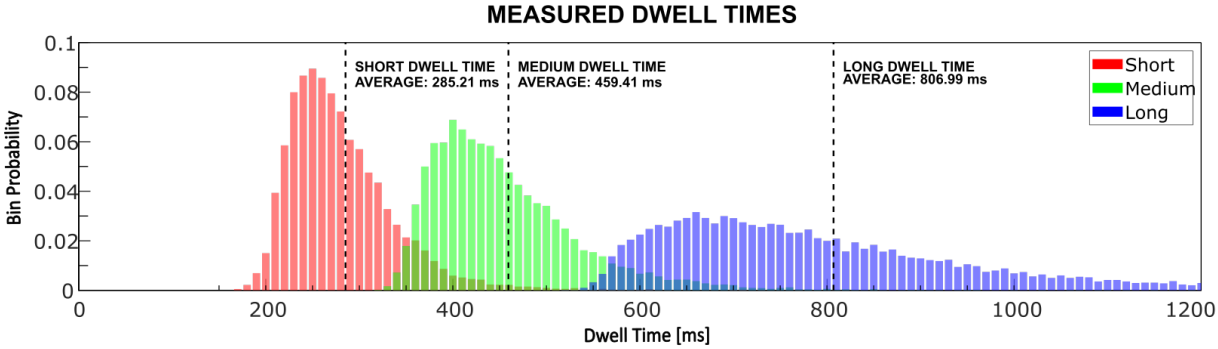

Figure 4. Visual Lead-in Dwell Time Histogram Plots. These show the distribution of measured dwell times executed by participants in the three experimental dwell time conditions. The black dotted line indicates the mean for each dwell time condition.

Hand Trajectories. The hand trajectories for all three conditions in the Visual Lead-in Experiment 1 were examined in four different stages of the experiments (Fig. 5). The first column (Last Null) shows hand trajectories during the last block of trials in the null phase and shows that participants were able to perform unhindered straight movements in all three conditions. The second column (Initial Curl) shows the first block of trials after the introduction of the curl-field, revealing that participants deviated strongly from a straight movement in all three conditions. The third column (Final Curl) shows hand trajectories during the last block of curl-field trials. This highlights distinct differences across dwell time conditions. Notably, in the short dwell time condition, participants performed almost straight movements, close to baseline performance. In the medium dwell time condition, participants still exhibited effects of the curl-fields and still deviated somewhat from the straight path. In the long dwell time condition, the effect of the curl-fields was still apparent, suggesting there was little adaptation. The final column (Washout) shows the first block of trials during the washout phase, after the curl-field was removed. It is evident that short dwell times led to strong aftereffects, leading to significant deviation from straight trajectories in the opposite direction to that seen during curl-field exposure. As the dwell time increased, the deviation was reduced, and in the long dwell time condition, the trajectories were effectively straight.

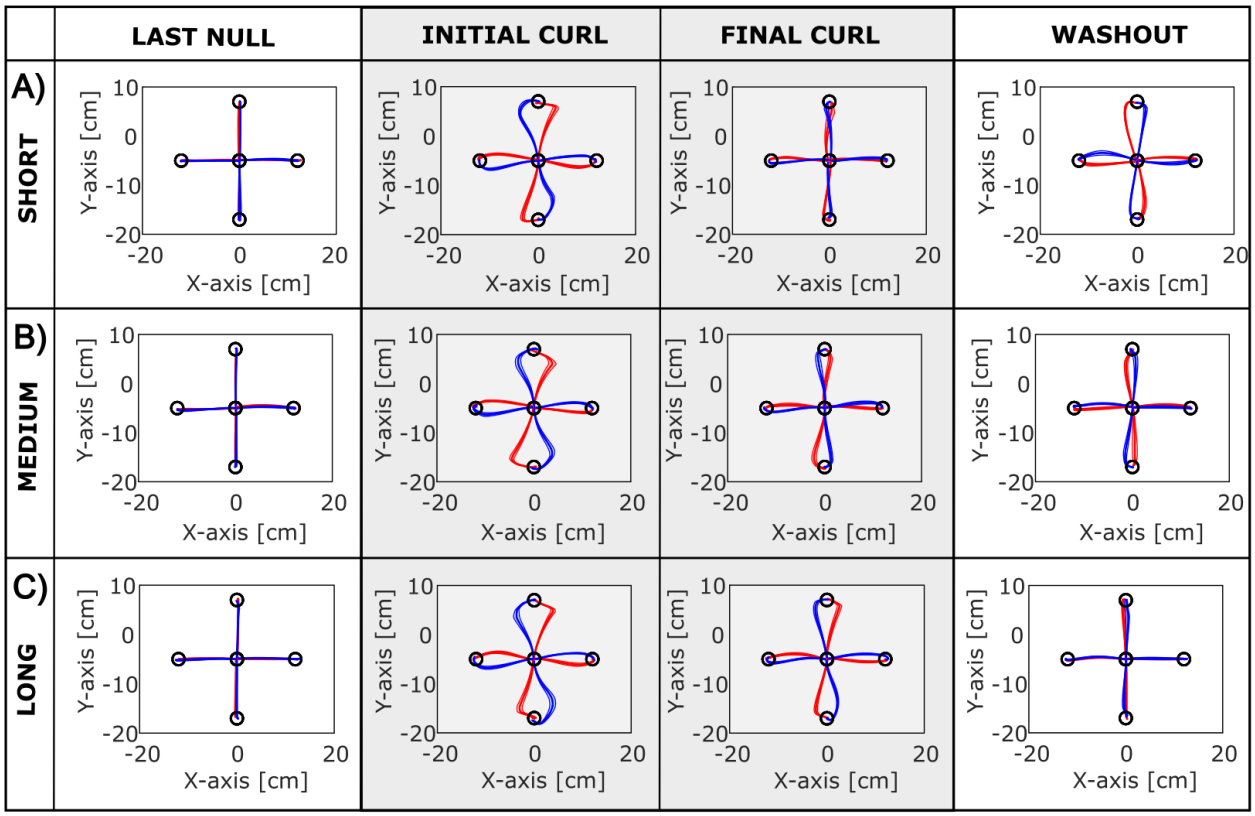

Figure 5. Hand Trajectories in the Visual Lead-in Experiment 1. The solid thick lines indicate the mean across participants and the shaded region indicates the standard error of the mean. Red colors indicate trajectories in the context associated with CW curl force fields whereas blue colors indicate the trajectories in the context associated with CCW curl force fields. **A:** The short dwell time condition. **B:** The medium dwell time condition. **C:** The long dwell time condition. The columns represent the Last Null, Initial Curl, Final Curl, and Washout stages of the experiment.

Kinematic Error and Force Compensation: To examine the overall level of adaptation in the different dwell conditions, we initially combined the effect of both curl-field directions by calculating a single value from the dual Maximum Perpendicular Error (MPE) and compensation values (Fig. 6).

To examine kinematic error during the experiments we plotted the Maximum Perpendicular Error (MPE) across the experimental blocks for the short, medium, and long dwell time conditions (Fig. 6A). During the null-field exposure, MPE was essentially zero across all conditions. Upon the introduction of the curl-field, MPE dramatically increases in all three conditions. However, by the end of curl-field exposure, MPE decreases by a larger amount in the case of short dwell times compared to long dwell times. In this case, MPE for the medium dwell time was only slightly lower that for the longer dwell times. During the final washout phase, the MPE exhibited a negative sign,

indicating deviation in the opposite direction of that created by the curl-field. Short Dwell times led to a larger magnitude of after effect than medium or long dwell times.

Repeated measures ANOVAs indicated that the MPE showed significant variations between the pre-exposure, initial exposure, final exposure, and washout phases for all dwell time conditions. Post-hoc comparisons further tested the significant differences between these phases. In the short dwell time condition ($F_{3,21}$ = 121.748; $p < 0.001$; $\omega^2 = 0.903$), MPE was low during the initial null-field exposure, then it significantly increased upon introduction of the curl-field ($p_{bonf} < 0.001$). Over the exposure phase, MPE significantly decreased ($p_{bonf} < 0.001$). MPE during the washout phase showed a significant difference compared to the pre-exposure phase ($p_{bonf} < 0.001$). For the medium dwell time condition ($F_{3,21}$ = 176.789; $p < 0.001$; $\omega^2 = 0.929$), MPE was low during the initial null-field exposure, and MPE increased significantly upon the introduction of the curl-field ($p_{bonf} < 0.001$). Over the exposure phase, MPE decreased significantly ($p_{bonf} < 0.001$). MPE during the washout phase showed a significant difference compared to the pre-exposure phase ($p_{bonf} = 0.007$). In the long dwell time condition ($F_{3,21}$ = 220.335; $p < 0.001$; $\omega^2 = 0.926$), MPE increased significantly upon the introduction of the curl-field ($p_{bonf} < 0.001$). Over the exposure phase, MPE decreased significantly ($p_{bonf} < 0.001$). However, MPE during the washout phase showed no significant difference compared to the pre-exposure phase ($p_{bonf} = 0.669$).

To quantify the amount of predictive force compensation to the force fields, we examined the force compensation on the channel trials for the short, medium and long conditions (Fig. 6B). During the initial null-field exposure, compensation was low in all dwell time conditions. Upon the introduction of the curl-field, compensation continued to increase slowly over the whole exposure period. By the end of the curl-field exposure, the compensation for the short dwell time condition increased the most, while for longer dwell times, the least compensation was observed. An intermediate compensation level was seen for the medium dwell time. During the washout phase, compensation values decayed in all three dwell time conditions. Repeated measures ANOVAs indicated a significant increase in force compensation between the final pre-exposure and final exposure levels for short dwell times ($F_{1,7}$ = 59.253; $p < 0.001$; $\omega^2 = 0.785$), medium dwell times ($F_{1,7}$ = 28.357; $p = 0.001$; $\omega^2 = 0.617$), and long dwell times ($F_{1,7}$ = 8.366; $p = 0.023$; $\omega^2 = 0.280$).

The MPE and compensation results indicate that participants were better able to compensate opposing dynamics by making use of the visual lead-in context at shorter dwell times. The contextual effect decreased as the dwell time increased. Observations from the trajectory plots (Fig. 5) are consistent with these findings.

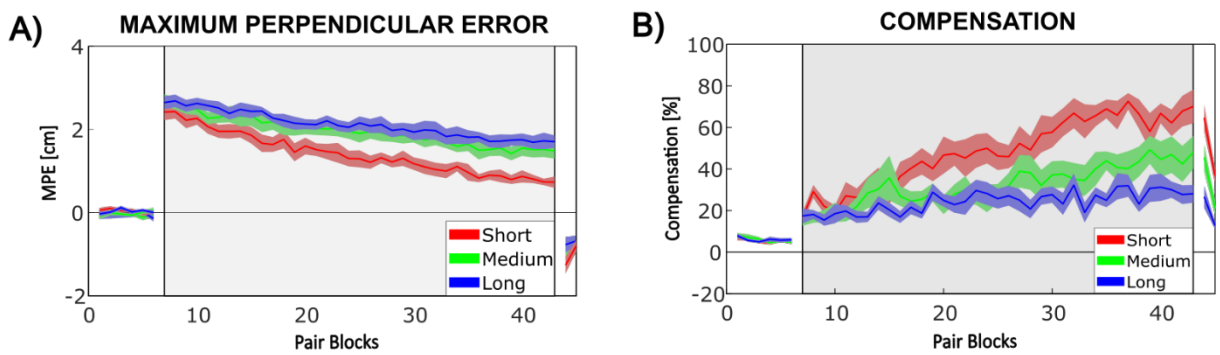

Figure 6. Adaptation in the Visual Lead-In Experiment 1. **A:** Kinematic error. Overall Mean (solid line) ± SE (shaded region) of the MPE plotted against block pairs for the short, medium, and long dwell-time conditions. **B:** Force Compensation. Overall Mean ± SE percentage of compensation for the short, medium, and long dwell-time conditions.

Independent Adaptation to Opposing Force Fields: While the previous analysis clearly shows adaptation to the dynamics, it is unclear the level to which this is independently adapted to each force field direction. Fig. 7 shows the Maximum Perpendicular Error (MPE) and compensation for the Visual Lead-In Experiment 1, with both plotted separately for the two contextual directions, to permit the individual examination of the learning process in each curl-field direction. Similar trends are observed in both curl-field directions.

We compared the final exposure MPE in both curl-field directions of block pairs across participants (Fig. 7A). A repeated measures ANOVA indicated that there were no significant differences between the two directions for the short dwell time condition ($F_{1,7}$ = 1.199; p = 0.310; ω² = 0.004), for the medium dwell time condition ($F_{1,7}$ = 0.246; p = 0. 645; ω² = 0.000), or for the long dwell time condition ($F_{1,7}$ = 3.501; p = 0.104; ω² = 0.034).

Similarly, Fig. 7B shows the mean ± SE compensation for short, medium, and long dwell times. We compared the final exposure compensation in both curl-field directions of block pairs across participants. A repeated measures ANOVA indicated that they were not significantly different, for the short dwell time condition ($F_{1,7}$ = 0.023; p = 0.883; ω² = 0.000), for the medium dwell time condition ($F_{1,7}$ = 0.131; p = 0.728; ω² = 0.000), or for the long dwell time condition ($F_{1,7}$ = 3.501; p = 0.433; ω² = 0.000).

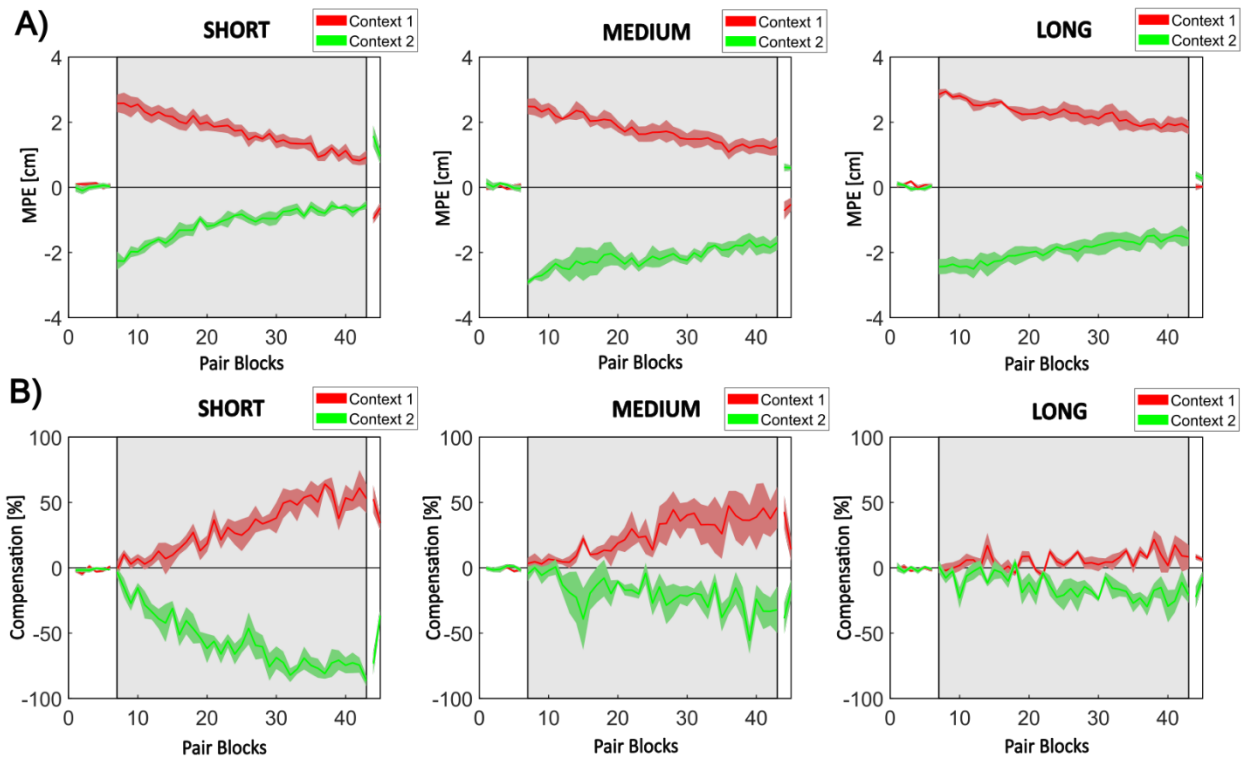

Figure 7. Independent Adaptation to Opposing Force Fields. Visual Lead-In Mean ± SE Maximum Perpendicular Error (MPE) and Compensation are plotted for both opposing curl-fields. **A:** Mean ± SE MPE for short, medium, and long dwell times. **B:** Mean ± SE compensation for short, medium, and long dwell times.

Passive Lead-in Experiment 2:

Dwell Time Analysis: Dwell times were different across the three conditions in the passive lead-in experiment (Fig. 8). For the short, medium, and long dwell time conditions, the mean ± SE values were 317 ± 13.4ms, 528.9 ± 5.1ms, and 818.7 ± 5.6ms, respectively. In addition, the distributions spread out more as the dwell time increases. In the short condition, the mean and mode values deviate and are shifted away from the mean to the left of the mean. However, by the long condition, the mode and mean times are much closer and the distributions become more symmetrical about the mean.

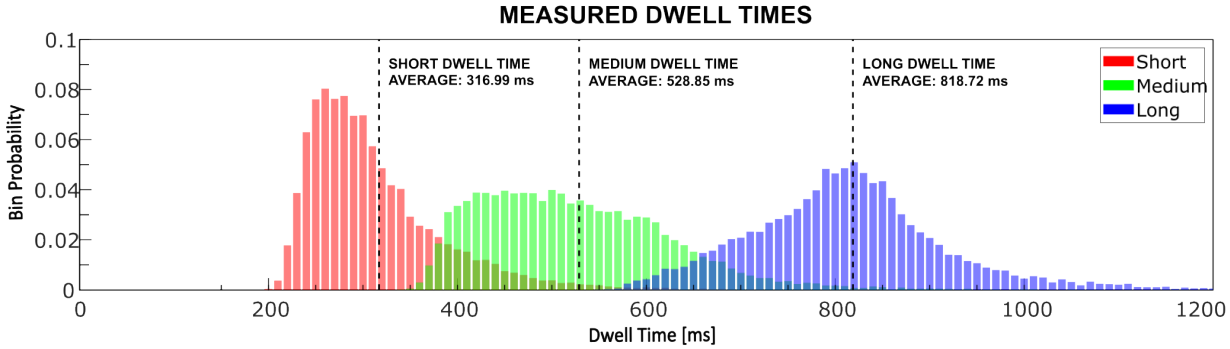

Figure 8. Passive Lead-in Dwell Time Histogram Plots. Histograms show the distribution of measured movement dwell times in the lead-in movements executed by participants in the three experimental dwell time conditions. The black dotted line indicates the mean in each dwell time condition.

Hand Trajectories: Hand trajectories were computed across the four stages for each of the three dwell time conditions (Fig. 9). As shown in the first column (Last Null), participants were able to perform unhindered straight movements in all three dwell time conditions. The second column (Initial Curl) shows that on initial curl-field exposure, participants deviated strongly from a straight movement in all three conditions. The third column (Final Curl) shows that by the end of the training phase, participants' hand movements were almost straight in the short dwell time condition but deviated more from a straight line as the dwell time increased. However, even in the long dwell time condition, they were still straighter than those seen in the initial exposure phase. The final column (Washout) shows strong aftereffects for the short dwell time condition. As the dwell time increases, aftereffects become less prominent although there is still some deviation from a straight-line trajectory even in the long dwell time condition.

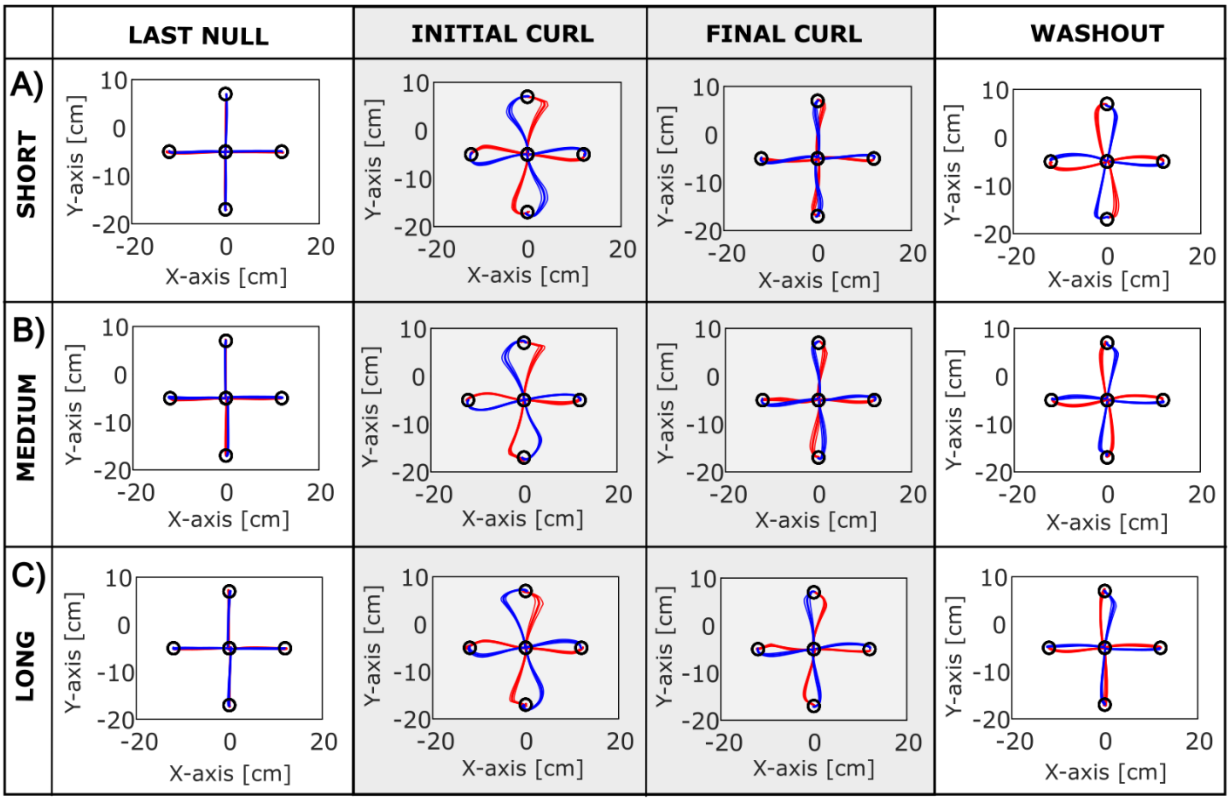

Figure 9. Hand Trajectories for the Passive Lead-In Experiment. Plot of the Mean ± SE Hand Trajectories for the three experiment conditions. **A:** The short dwell time condition. **B:** The medium dwell time condition. **C:** The long dwell time condition. The columns represent the Last Null, Initial Curl, Final Curl, and Washout stages of the experiment.

Kinematic Error and Force Compensation:

To combine the effect of both curl-field directions, we calculated a single value from the dual Maximum Perpendicular Error (MPE) and compensation values (Fig. 10). Fig. 10A shows the Mean ± SE Maximum Perpendicular Error (MPE) for the short, medium, and long dwell time conditions. During the null-field exposure, MPE was essentially zero across all conditions. Upon the introduction of the curl-field, MPE dramatically increased in all three conditions. By the end of curl-field exposure, MPE decreased more with shorter dwell times than with longer dwell times. During the washout phase, the MPE exhibited a negative value.

Repeated measures ANOVAs revealed significant differences in MPE across the pre-exposure, initial exposure, final exposure, and washout phases for all dwell time conditions. In the short dwell time condition, significant variations were observed ($F_{3,21}$ = 134.537, $p < 0.001$, $\omega^2 = 0.909$). Post-hoc comparisons showed that MPE was low during the initial null-field exposure but increased significantly upon the introduction of the curl-field ($p_{bonf} < 0.001$). Over the exposure phase, MPE decreased significantly ($p_{bonf} < 0.001$), and during the washout phase, MPE showed a significant difference compared to pre-exposure ($p_{bonf} < 0.001$). In the medium dwell time condition, MPE also showed significant differences across the phases ($F_{3,21}$ = 186.893, $p < 0.001$, $\omega^2 = 0.924$). During the initial null-field exposure, MPE was low, but it increased significantly with the introduction of the curl-field ($p_{bonf} < 0.001$). MPE decreased significantly over the exposure phase ($p_{bonf} < 0.001$), and in the washout phase, MPE remained significantly different from the pre-exposure phase ($p_{bonf} = 0.002$). For the long dwell time condition, significant variations were found ($F_{3,21}$ = 101.650, $p < 0.001$, $\omega^2 = 0.889$). MPE was initially low during the null-field exposure and increased significantly with the curl-field introduction ($p_{bonf} < 0.001$). Over the exposure phase, MPE decreased significantly ($p_{bonf} = 0.002$), and the washout phase showed a significant difference in MPE compared to the pre-exposure phase ($p_{bonf} = 0.026$).

Again, the mean force compensation was examined (Fig. 10B) for the short, medium, and long dwell time conditions. During the initial null-field exposure, compensation was low in all dwell time conditions. Upon the introduction of the curl-field, compensation began to increase. By the end of the curl-field exposure, the compensation had increased for all dwell time conditions, but less so as dwell time increased. During the washout phase, compensation values decayed in all three dwell time conditions.

A repeated measures ANOVA indicated a significant increase in force compensation between the final pre-exposure and final exposure levels across all dwell time conditions. In the short dwell time condition, the increase was highly significant ($F_{1,7}$ = 182.743, $p < 0.001$, $\omega^2 = 0.929$). For the medium dwell time condition, a significant increase in force compensation was also observed ($F_{1,7}$ = 30.547, $p < 0.001$, $\omega^2 = 0.664$). Similarly, in the

long dwell time condition, a significant increase in force compensation between the final pre-exposure and final exposure levels was found ($F_{1,7}$ = 39.970, p < 0.001, ω² = 0.693).

These MPE and force compensation results demonstrate that participants using passive lead-in contexts could effectively compensate for both opposing curl-field directions, consistent with the raw trajectory plots shown in Fig. 9. Although the contextual effect diminished as the dwell time increased, it decreased less than what was observed in Visual Lead-in Experiment 1.

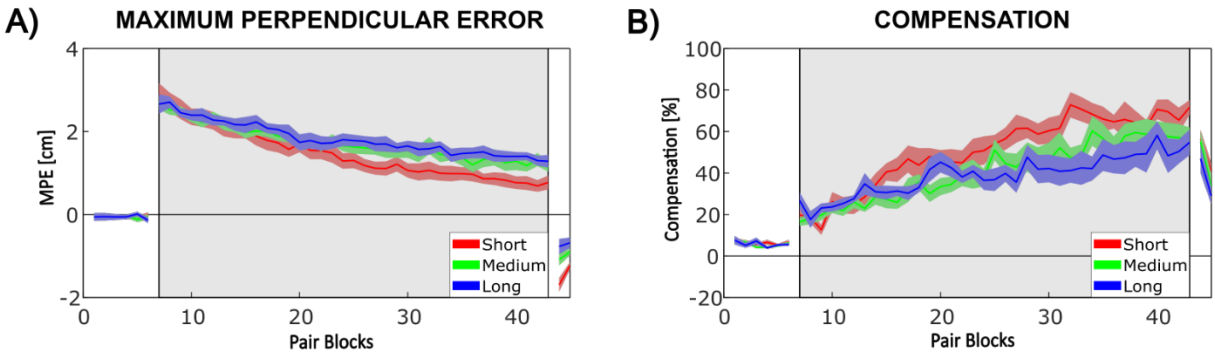

Figure 10. MPE and Compensation for the Passive Lead-in Experiment 2. **A:** Overall Mean ± SE MPE plotted against block pairs for each of the three dwell-time conditions. **B:** Overall Mean±SE percentage of compensation for each of the three dwell-time conditions.

Independent Adaptation to Opposing Force Fields: Fig. 11 shows the Maximum Perpendicular Error (MPE) and compensation for the Passive Lead-In Experiment 2, for both plotted separately for the two curl-field directions. These were again examined to test if there are differences in the adaptation of the two field directions.

Fig. 11A shows the Mean ± SE Maximum Perpendicular Error (MPE) for the short, medium, and long dwell time conditions. Similar trends are seen in both curl-field directions. We compared the final exposure MPE across participants for both curl-field directions within block pairs. A repeated measures ANOVA indicated that there were no significant differences in adaptation across curl-field directions for the short, medium and long dwell time condition. Their analyses yielded the following statistics: ($F_{1,7}$ = 0.231; p = 0. 645; ω² = 0.000), ($F_{1,7}$ = 3.543; p = 0. 102; ω² = 0.072), and ($F_{1,7}$ = 2.178; p = 0. 184; ω² = 0.059) respectively. That is, participants adapted equally to both force field directions.

Fig. 11B shows the mean ± SE compensation values for short, medium, and long dwell times. We compared the final exposure compensation in both curl-field directions of block pairs across participants. A repeated measures ANOVA indicated that there were no significant differences for the medium and long dwell time conditions $F_{1,7}$ = 0.268; p = 0.

621; ω² = 0.000) and ($F_{1,7}$ = 2.780; p = 0. 139; ω² = 0.067) respectively). However, a significant difference was observed in the short dwell time condition ($F_{1,7}$ = 6.078; p = 0. 043; ω² = 0.210).

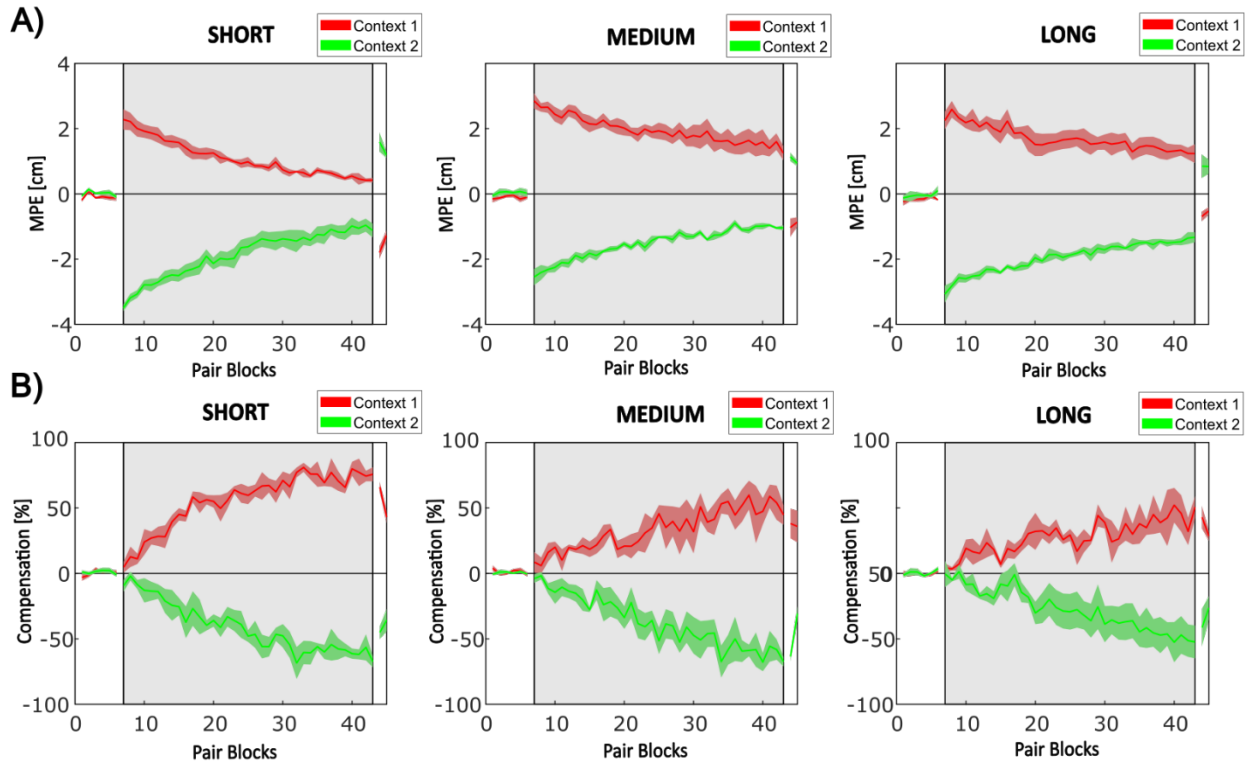

Figure 11. Independent Adaptation to Opposing Force Fields for the Passive Lead-In. The mean ± SE MPE and force compensation for both opposing curl-fields. **A:** Mean ± SE MPE for short, medium, and long dwell times. **B:** Mean ± SE compensation for short, medium, and long dwell times.

Comparison of Results Across Experiments

To contrast the adaptation across the two experiments we performed comparisons of the levels of curl-field compensation achieved in both the Visual Lead-in Experiment 1 and Passive Lead-in Experiment 2 (Fig. 12). At short dwell times (Fig. 12A), compensation levels increased similarly in both experiments during curl-field exposure. At medium dwell times (Fig. 12B), a slight divergence emerged, with the Visual Lead-in Experiment 1 showing a slower increase in learning than in the Passive Lead-in Experiment 2. This difference became more pronounced at long dwell times (Fig.12C), where the Visual Lead-in Experiment 1 exhibited noticeably less learning than the Passive Lead-in Experiment 2.

To explore these trends, the mean compensation values over the last 10 blocks of curl-field exposure trials were plotted against the measured dwell times (Fig. 12D). This highlights a clear contrast between the two experiments. In the Visual Lead-in Experiment 1, compensation declined as dwell time increased, while the Passive Lead-in Experiment

2 maintained higher compensation levels regardless of dwell time. A detailed breakdown of the compensation, MPE, and dwell time values for the last 10 blocks of exposure trials is provided in Table 2.

Table 2. Measured average dwell times over the entire experiment and compensation values over the last 10 blocks of exposure trials for the visual and passive lead-In conditions (mean±SE).

	Visual Lead-In Experiment 1		**Passive Lead-in Experiment 2**	
	COMP	**DWELL TIME**	**COMP**	**DWELL TIME**
Short	65.076 ± 6.019%	285.2 ± 8.5ms	67.733 ± 3.996%	317.0 ± 13.4ms
Medium	40.771 ± 9.497%	459.4 ± 7.6ms	56.147 ± 6.297%	528.9 ± 5.1ms
Long	15.553 ± 4.102%	807.0 ± 20.6ms	47.811 ±.6.958%	818.7 ± 5.6ms

An ANOVA analysis of the last 10 curl-field exposure trials was performed for both the Visual Lead-In Experiment 1 and the Passive Lead-In Experiment 2. Final exposure compensation showed significant variations between dwell-time conditions (F_2 = 14.685; $p < 0.001$; $\omega^2 = 0.311$) and experimental conditions (F_1 = 10.257; p =0.003; $\omega^2 = 0.105$). Post-hoc comparisons revealed no significant differences between visual experiment 1 and passive experiment 2 experiments for short and medium dwell times (p_{bonf} =1.000). However, there was a significant difference for long dwell times (p_{bonf} =0.014).

We note that, even though passive generally exhibited longer mean dwell time values than in the visual modality, we still saw a significantly greater adaptation in the Passive lead-in Experiment 2 than in the Visual Lead-in Experiment 1. This indicates that it is the form of the lead-in modality that is responsible for the observed differences in adaptation achieved, since the Passive Lead-in Experiment 2 showed greater adaptation even though the dwell times were slightly longer in comparable conditions.

These findings indicate a more rapid decay of contextual effectiveness when using visual lead-in cues compared to passive lead-ins. Furthermore, the data suggest that the effectiveness of visual lead-in cues substantially reduces when dwell times exceed approximately 800ms.

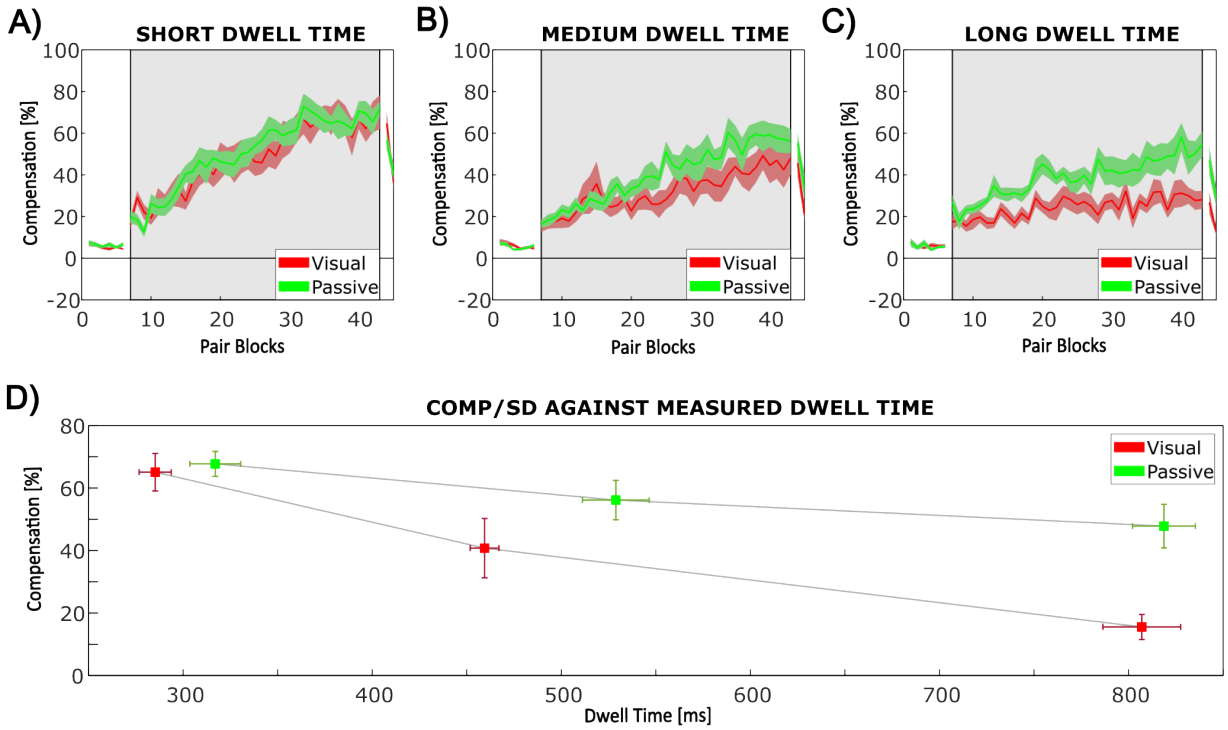

Figure 12. Comparison of adaptation across the experiments. Plot of mean±SE compensation values for the Visual Lead-in Experiment 1 and the Passive Lead-in Experiment 2 contexts across the three different dwell time conditions. **A:** Plot of compensation against block pairs for both experiments at short dwell times. **B:** Plot of compensation against block pairs for both experiments at medium dwell times. **C:** Plot of compensation against block pairs for both experiments at long dwell times. **D:** Final level of curl-field compensation (mean±SE) plotted against the measured dwell time (mean±SE) for both experiments.

DISCUSSION (1178/1500)

Summary

Using an interference paradigm, we investigated the contextual effects of visual and passive lead-in movements as a function of dwell time. Our results revealed significant differences between the two experimental conditions. We found that in both lead-in modalities, the level of adaptation achieved decreased as dwell time increased. However, visual lead-in movements showed a greater decline compared to passive lead-in movements. Although adaptation in both visual and passive lead-in conditions was similar at shorter dwell times, recall with visual lead-ins became much smaller as dwell time exceeded approximately 800ms. In contrast, significantly more adaptation was present in the passive lead-in condition.

These results align with and extend previous research on the behavior of active lead-in contextual movements, which demonstrated a falloff of the contextual effect and a subsequent reduction in adaptation as dwell time increased (14). In this former study, it was found that active lead-ins led to compensation levels 44.4%, 34.3%, and 7.9%, at measured dwell times of 246 ± 7.5ms, 680 ± 13.1ms, and 1211 ± 26.3ms, respectively. These values are slightly less than the ones achieved here (see Table 2), but the trend is still similar.

Differences in the generalization characteristics of memory recall between past visual and passive lead-in movements are well-documented. In particular, training with passive lead-in movements at a given angular direction transfers to other angular directions over a narrow range, with tuning exhibiting a Gaussian-shaped response with a standard deviation of about 43° (15). In contrast, visual lead-in movements display a weaker and broader angular generalization, with a standard deviation of about 264° (17). Additionally, the generalization of passive and visual lead-in movements also differs in terms of movement speed and duration, with passive lead-in movements exhibiting slightly narrower generalization characteristics than visual lead-in movements (18). These differences in generalization characteristics suggest that visual and passive lead-in movements are processed differently in the formation and selection of motor memories.

Visual and Proprioceptive Feedback

The control of visually guided arm movements, including the point-to-point movements examined in this study, generally involves integrating visual and proprioceptive sensory feedback within the brain.

The generation of volitional arm movement involves multiple brain areas that integrate visual and proprioceptive feedback to coordinate precise motor control. In the cerebral cortex, both the premotor cortex (PMC) and the supplementary motor area (SMA) play key roles in planning and preparing movements, using visual and proprioceptive inputs to adjust and refine the action (34, 35). The primary motor cortex (M1) is crucial for initiating and executing voluntary movements, sending direct signals to the muscles (36). The posterior parietal cortex (PPC) integrates sensory information, particularly visual and proprioceptive inputs, and contributes to motor planning in the PMC and SMA (37).

Additionally, other brain regions are involved in movement. The cerebellum is vital for fine-tuning and ensuring the smooth execution of movements, while the basal ganglia contribute to movement regulation and the selection of appropriate motor strategies. Both the cerebellum and the basal ganglia rely on both types of sensory feedback to optimize motor output. See Krakauer et al.for a general overview of motor learning, control, and brain region involvement (38).

Visual information requires complex processing in the visual cortex and higher brain centers, introducing delays and potential degradation over time (39–41). In visually guided movements, vision provides not only the location of the desired target, but also an online indication of limb position and movement (42). Such visual feedback is essential

for planning and guiding movements over extended time scales. However, visual feedback experiences delays of approximately 100 to 150 milliseconds due to the extensive processing required in the visual cortex and higher brain centers (43, 44).

In contrast, proprioceptive information, which originates from sensors in the muscle fibers, tendons, and joints, is transmitted much faster (45). This is because proprioceptive pathways are shorter and involve more direct processing, resulting in delays of approximately 30 to 50 milliseconds (46). Proprioception provides continuous, lower-latency feedback about the body's position and movement (45, 47). Such proprioceptive feedback is crucial for rapid, reflexive compensatory movements, and multi-joint control, as is clearly demonstrated in patients who experience deficits in proprioception (48).

Thus, visual feedback has a longer time delay compared to proprioceptive feedback, primarily due to the extended time required to process signals in the visual cortex and their subsequent integration into higher brain centers (49). In general, sensory feedback delays can vary between 30 and 250 milliseconds (50, 51). These differences in delay times significantly influence how each type of feedback is utilized in motor control. Effective motor control typically requires the integration of both types of feedback, visual and proprioceptive, to achieve satisfactory performance in various tasks.

It is known that humans can integrate visual and haptic information for the purpose of perception (52) and are able to utilize of this to guide the generation of movement (53). However, it has also been shown that during movement, healthy humans primarily rely on dynamic estimates of hand motion derived from limb afferent feedback, even when visual information about limb movement is accessible (54). It was proposed that this is the case because the nervous system takes into account both sensory variances and temporal delays to achieve optimal multisensory integration and feedback control. Therefore, there is a bias towards using the proprioceptive signals rather than the visual signals, due to the former’s shorter latency.

The Relevance of Visual and Proprioceptive Feedback

As well as differences in time delays between different modalities of sensory input, other sources of uncertainty might arise due to the phenomena they are sensing. Visual feedback depends on observations made in the environment and is affected by external environmental conditions, such as levels of illumination, which can change rapidly and unpredictably. Importantly, visual feedback not only corresponds to movement feedback from arm movements, but also from other movements in the environment. Consequently, much visual information may only be indirectly relevant for motor control purposes. As a general principle, is it known that exposure to a more variable range of experiences affects and widens generalization (55). Thus, a broader range of visual experience is consistent with the wider and shallower generalization characteristic seen for visual lead-in movements.

In contrast, proprioceptive information arises internally within the body, making it directly related to arm movement. It is also less susceptible to external environmental changes,

making it task-relevant and reliable. Thus, there is more inherent processing delay in the visual pathway, and visual information may arise from multiple observations in the environment. By comparison, the proprioceptive pathway has a shorter inherent delay and relates more directly to the state of the arm. As time delay increases, uncertainty in the relevance of feedback will increase, but more in the case of visual input than in proprioceptive input. This hypothesis would also explain why the directional tuning observed for visual contextual lead-in movements was so wide compared to that of passive movements (15, 17). In the visual condition, there will simply be more uncertainty about the prior movement direction due to the longer processing delay and the observational uncertainty arising from the nature of the environment.

DISCLOSURES

The authors declare that they have no financial, personal, or professional conflicts of interest that could have influenced the content of this paper.

AUTHOR CONTRIBUTIONS

LAH, ISH, and DWF conceived and designed the study. ISH implemented the study on the vBOT, and LAH conducted the data collection. Both LAH and ISH carried out the data analysis. LAH and ISH wrote the initial draft of the manuscript. All three authors, LAH, ISH, and DWF, reviewed and edited the manuscript.

REFERENCES

1. **Shadmehr R**, **Mussa-Ivaldi FA**. Adaptive representation of dynamics during learning of a motor task. *J Neurosci* 14: 3208–3224, 1994. doi: 10.1523/JNEUROSCI.14-05-03208.1994.

2. **Thoroughman KA**, **Shadmehr R**. Learning of action through adaptive combination of motor primitives. *Nature* 407: 742–747, 2000. doi: 10.1038/35037588.

3. **Nozaki D**, **Kurtzer I**, **Scott SH**. Limited transfer of learning between unimanual and bimanual skills within the same limb. *Nat Neurosci* 9: 1364–1366, 2006. doi: 10.1038/nn1785.

4. **Shadmehr R**, **Brashers-Krug T**. Functional stages in the formation of human long-term motor memory. *J Neurosci Off J Soc Neurosci* 17: 409–419, 1997. doi: 10.1523/JNEUROSCI.17-01-00409.1997.

5. **Krakauer JW**, **Mazzoni P**. Human sensorimotor learning: Adaptation, skill, and beyond. *Curr Opin Neurobiol* 21: 636–644, 2011. doi: 10.1016/j.conb.2011.06.012.

6. **Zarahn E**, **Weston GD**, **Liang J**, **Mazzoni P**, **Krakauer JW**. Explaining Savings for Visuomotor Adaptation: Linear Time-Invariant State-Space Models Are Not Sufficient. *J Neurophysiol* 100: 2537–2548, 2008. doi: 10.1152/jn.90529.2008.

7. **Sing GC**, **Smith MA**. Reduction in Learning Rates Associated with Anterograde Interference Results from Interactions between Different Timescales in Motor Adaptation. *PLOS Comput Biol* 6: e1000893, 2010. doi: 10.1371/journal.pcbi.1000893.

8. **Hamel R**, **Lepage J**, **Bernier P**. Anterograde interference emerges along a gradient as a function of task similarity: A behavioural study. *Eur J Neurosci* 55: 49–66, 2022. doi: 10.1111/ejn.15561.

9. **Brashers-Krug T**, **Shadmehr R**, **Bizzi E**. Consolidation in human motor memory. *Nature* 382: 252–255, 1996.

10. **Gandolfo F**, **Mussa-Ivaldi FA**, **Bizzi E**. Motor learning by field approximation. *Proc Natl Acad Sci* 93: 3843–3846, 1996. doi: 10.1073/pnas.93.9.3843.

11. **Krakauer JW**, **Ghilardi MF**, **Ghez C**. Independent learning of internal models for kinematic and dynamic control of reaching. *Nat Neurosci* 2: 1026–1031, 1999. doi: 10.1038/14826.

12. **Karniel A**, **Mussa-Ivaldi FA**. Does the motor control system use multiple models and context switching to cope with a variable environment? *Exp Brain Res* 143: 520–524, 2002. doi: 10.1007/s00221-002-1054-4.

13. **Caithness G**, **Osu R**, **Bays P**, **Chase H**, **Klassen J**, **Kawato M**, **Wolpert DM**, **Flanagan JR**. Failure to consolidate the consolidation theory of learning for sensorimotor adaptation tasks. *J Neurosci Off J Soc Neurosci* 24: 8662–8671, 2004. doi: 10.1523/JNEUROSCI.2214-04.2004.

14. **Howard IS**, **Ingram JN**, **Franklin DW**, **Wolpert DM**. Gone in 0.6 Seconds: The Encoding of Motor Memories Depends on Recent Sensorimotor States. *J Neurosci* 32: 12756–12768, 2012. doi: 10.1523/JNEUROSCI.5909-11.2012.

15. **Howard IS**, **Franklin DW**. Neural Tuning Functions Underlie Both Generalization and Interference. *PloS One* 10: e0131268, 2015. doi: 10.1371/journal.pone.0131268.

16. **Sarwary M**, **Stegeman D**, **Selen L**, **Medendorp P**. Generalization and transfer of contextual cues in motor learning. *J Neurophysiol* 114: jn.00217.2015, 2015. doi: 10.1152/jn.00217.2015.

17. **Howard IS**, **Franklin DW**. Adaptive tuning functions arise from visual observation of past movement. *Sci Rep* 6, 2016. doi: 10.1038/srep28416.

18. **Howard IS**, **Franklin S**, **Franklin DW**. Asymmetry in kinematic generalization between visual and passive lead-in movements are consistent with a forward model in the sensorimotor system. *PLOS ONE* 15: e0228083, 2020. doi: 10.1371/journal.pone.0228083.

19. **Gippert M**, **Leupold S**, **Heed T**, **Howard IS**, **Villringer A**, **Nikulin VV**, **Sehm B**. Prior Movement of One Arm Facilitates Motor Adaptation in the Other. *J Neurosci* 43: 4341–4351, 2023. doi: 10.1523/JNEUROSCI.2166-22.2023.

20. **Howard IS**, **Franklin S**, **Franklin DW**. Kernels of Motor Memory Formation: Temporal Generalization in Bimanual Adaptation. .

21. **Franklin S**, **Leib R**, **Dimitriou M**, **Franklin DW**. Congruent visual cues speed dynamic motor adaptation. *J Neurophysiol* 130, 2023. doi: 10.1152/jn.00060.2023.

22. **Howard IS**, **Ford C**, **Cangelosi A**, **Franklin DW**. Active lead-in variability affects motor memory formation and slows motor learning. *Sci Rep* 7, 2017. doi: 10.1038/s41598-017-05697-z.

23. **Oldfield RC**. The assessment and analysis of handedness: The Edinburgh inventory. *Neuropsychologia* 9: 97–113, 1971. doi: 10.1016/0028-3932(71)90067-4.

24. **Howard IS**, **Ingram JN**, **Wolpert DM**. A modular planar robotic manipulandum with end-point torque control. .

25. **Gandolfo F**, **Mussa-Ivaldi FA**, **Bizzi E**. Motor learning by field approximation. *Proc Natl Acad Sci* 93: 3843–3846, 1996. doi: 10.1073/pnas.93.9.3843.

26. **Proud K**, **Heald JB**, **Ingram JN**, **Gallivan JP**, **Wolpert DM**, **Flanagan JR**. Separate motor memories are formed when controlling different implicitly specified locations on a tool. *J Neurophysiol* 121: 1342–1351, 2019. doi: 10.1152/jn.00526.2018.

27. **Scheidt R**, **Reinkensmeyer D**, **Conditt M**, **Rymer W**, **Mussa-Ivaldi F**. Persistence of Motor Adaptation During Constrained, Multi-Joint, Arm Movements. *J Neurophysiol* 84: 853–62, 2000. doi: 10.1152/jn.2000.84.2.853.

28. **Sadeghi M**, **Ingram J**, **Wolpert D**. Adaptive coupling influences generalization of sensorimotor learning. *PLOS ONE* 13: e0207482, 2018. doi: 10.1371/journal.pone.0207482.

29. **Orschiedt J**, **Franklin DW**. Learning context shapes bimanual control strategy and generalization of novel dynamics. *PLOS Comput Biol* 19: e1011189, 2023. doi: 10.1371/journal.pcbi.1011189.

30. **Smith MA**, **Ghazizadeh A**, **Shadmehr R**. Interacting Adaptive Processes with Different Timescales Underlie Short-Term Motor Learning. *PLOS Biol* 4: e179, 2006. doi: 10.1371/journal.pbio.0040179.

31. **Burdet E**, **Osu R**, **Franklin DW**, **Milner TE**, **Kawato M**. The central nervous system stabilizes unstable dynamics by learning optimal impedance. *Nature* 414: 446–449, 2001. doi: 10.1038/35106566.

32. **Milner TE**, **Franklin DW**. Impedance control and internal model use during the initial stage of adaptation to novel dynamics in humans. *J Physiol* 567: 651–664, 2005. doi: 10.1113/jphysiol.2005.090449.

33. **JASP Team, Version 0.19.1**. JASP. 2024.

34. **Hoshi E**, **Tanji J**. Distinctions between dorsal and ventral premotor areas: anatomical connectivity and functional properties. *Curr Opin Neurobiol* 17: 234–242, 2007. doi: 10.1016/j.conb.2007.02.003.

35. **Nachev P**, **Kennard C**, **Husain M**. Functional role of the supplementary and PRE-supplementary motor areas. *Nat Rev Neurosci* 9: 856–69, 2008. doi: 10.1038/nrn2478.

36. **Schieber MH**. Constraints on Somatotopic Organization in the Primary Motor Cortex. *J Neurophysiol* 86: 2125–2143, 2001. doi: 10.1152/jn.2001.86.5.2125.

37. **Andersen RA**, **Cui H**. Intention, Action Planning, and Decision Making in Parietal-Frontal Circuits. *Neuron* 63: 568–583, 2009. doi: 10.1016/j.neuron.2009.08.028.

38. **Krakauer JW**, **Hadjiosif AM**, **Xu J**, **Wong AL**, **Haith AM**. Motor learning. *Compr Physiol* 9: 613–663, 2019.

39. **Goodale MA**, **Milner AD**. Separate visual pathways for perception and action. *Trends Neurosci* 15: 20–25, 1992. doi: 10.1016/0166-2236(92)90344-8.

40. **Grill-Spector K**, **Malach R**. The human visual cortex. *Annu Rev Neurosci* 27: 649–77, 2004. doi: 10.1146/annurev.neuro.27.070203.144220.

41. **DiCarlo JJ**, **Zoccolan D**, **Rust NC**. How Does the Brain Solve Visual Object Recognition? *Neuron* 73: 415–434, 2012. doi: 10.1016/j.neuron.2012.01.010.

42. **Saunders JA**, **Knill DC**. Humans use continuous visual feedback from the hand to control fast reaching movements. *Exp Brain Res* 152: 341–352, 2003. doi: 10.1007/s00221-003-1525-2.

43. **Smeets J**, **Brenner E**. Fast corrections of movements with a computer mouse. *Spat Vis* 16: 365–376, 2003. doi: 10.1163/156856803322467581.

44. **Franklin DW**, **Wolpert DM**. Computational mechanisms of sensorimotor control. *Neuron* 72: 425–442, 2011. doi: 10.1016/j.neuron.2011.10.006.

45. **Proske U**, **Gandevia SC**. The Proprioceptive Senses: Their Roles in Signaling Body Shape, Body Position and Movement, and Muscle Force. *Physiol Rev* 92: 1651–1697, 2012. doi: 10.1152/physrev.00048.2011.

46. **Pruszynski JA**, **Kurtzer I**, **Scott SH**. The long-latency reflex is composed of at least two functionally independent processes. *J Neurophysiol* 106: 449–459, 2011. doi: 10.1152/jn.01052.2010.

47. **Moon KM**, **Kim J**, **Seong Y**, **Suh B-C**, **Kang K**, **Choe HK**, **Kim K**. Proprioception, the regulator of motor function. *BMB Rep* 54: 393–402, 2021. doi: 10.5483/BMBRep.2021.54.8.052.

48. **Sainburg RL**, **Poizner H**, **Ghez C**. Loss of proprioception produces deficits in interjoint coordination. *J Neurophysiol* 70: 2136–2147, 1993. doi: 10.1152/jn.1993.70.5.2136.

49. **Brenner E**, **van Straaten CAG**, **de Vries AJ**, **Baas TRD**, **Bröring KM**, **Smeets JBJ**. How the timing of visual feedback influences goal-directed arm movements: delays and presentation rates. *Exp Brain Res* 241: 1447–1457, 2023. doi: 10.1007/s00221-023-06617-6.

50. **Miall RC**, **Jackson J**. Adaptation to visual feedback delays in manual tracking: Evidence against the Smith Predictor model of human visually guided action. *Exp Brain Res Exp Hirnforsch Expérimentation Cérébrale* 172: 77–84, 2006. doi: 10.1007/s00221-005-0306-5.

51. **Cameron BD**, **de la Malla C**, **López-Moliner J**. The role of differential delays in integrating transient visual and proprioceptive information. *Front Psychol* 5: 50, 2014. doi: 10.3389/fpsyg.2014.00050.

52. **Ernst MO**, **Banks MS**. Humans integrate visual and haptic information in a statistically optimal fashion. *Nature* 415: 429–433, 2002. doi: 10.1038/415429a.

53. **Körding KP**, **Ku S**, **Wolpert DM**. Bayesian integration in force estimation. *J Neurophysiol* 92: 3161–3165, 2004. doi: 10.1152/jn.00275.2004.

54. **Crevecoeur F**, **Munoz DP**, **Scott SH**. Dynamic Multisensory Integration: Somatosensory Speed Trumps Visual Accuracy during Feedback Control. *J Neurosci Off J Soc Neurosci* 36: 8598–8611, 2016. doi: 10.1523/JNEUROSCI.0184-16.2016.

55. **Raviv L**, **Lupyan G**, **Green SC**. How variability shapes learning and generalization. *Trends Cogn Sci* 26: 462–483, 2022. doi: 10.1016/j.tics.2022.03.007.